Available online at www.sciencedirect.com
ScienceDirect
Journal of the European Ceramic Society 30 (2010) 1477–1482
www.elsevier.com/locate/jeurceramsoc

Nanoindentation with spherical tips of single crystals of YBCO textured by the Bridgman technique: Determination of indentation stress–strain curves

J.J. Roa [a,*], E. Jiménez-Piqué [b], X.G. Capdevila [a], M. Segarra [a]

[a] *Centro DIOPMA, Departamento de Ciencia de los Materiales e Ingeniería Metalúrgica, Instituto de Nanociencia y Nanotecnología de la Universidad de Barcelona (IN²UB), Facultat de Química, Universidad de Barcelona, Martí i Franquès 1, Barcelona E-08028, Spain*

[b] *Departamento de Ciencia de los Materiales e Ingeniería Metalúrgica, Universidad Politécnica de Cataluña, Diagonal 647 (ETSEIB), Barcelona E-08028, Spain*

Received 16 June 2009; received in revised form 15 October 2009; accepted 28 October 2009
Available online 16 December 2009

Abstract

The mechanical properties of superconductor ceramics are of interest in the manufacture of superconducting devices. The current trend is to produce smaller devices (using, e.g., thin films), and the correct characterization of small volumes of material is critical. Nanoindentation is used to assess mechanical parameters, and several studies determine hardness and Young's modulus by sharp indentation. However, studies on the elasto-plastic transition with spherical indentation are scare. Here we used, spherical diamond tip indenter experiments to explore the elasto-plastic transition and to measure the yield strength of the orthorhombic phase of $YBa_2Cu_3O_{7-\delta}$ (YBCO or Y-123) at room temperature. The study was carried out for a range of monodomains on the (1 0 1)-plane for Bridgman samples. Inspection of the load–unload curves for penetration depths lower than 200 nm allows for observation of the elasto-plastic transitions. Focused ion beam (FIB) trenches showed no cracking due to the indentation, although oxygenation cracks were apparent. The mean pressure for the onset of elasto-plastic deformation is 3.5 GPa, and the elastic modulus, E, calculated using the Hertzian equations is 123.5 ± 3.4 GPa.

Keywords: Superconducting; Nanoindentation; Stress–strain relationship

1. Introduction

The mechanical properties of YBCO superconducting ceramics are critical to the design of superconducting devices such as cables and motors. Precise knowledge of the elastic and deformation behaviour is a prerequisite for successful manufacturing and operation of such devices. However, very little information on the elastic-to-plastic transition is available in the literature.

The superconducting matrix of YBCO materials, $YBa_2Cu_3O_{7-\delta}$, (Y-123), contains a fine, well-dispersed distribution of Y_2BaCuO_5 (Y-211) precipitates. The Y-211 particles increase the irreversibility line by acting as pinning centres, improve crystal growth, and reduce macro-cracks.[1] The peritectic reaction is slow, so a fraction of non-reacted peritectic Y-211 can be retained in the final product in the form of inclusions with a size lower than few micrometers.[2]

The crystal of YBCO is highly anisotropic, as dislocations are confined to the (0 0 1) plane. Ledbetter et al.[3] reported that strong covalent and ionic bonds create high Peierls' barriers which constrain the dislocation mobility in YBCO single crystals. The incorporation of Y-211 particles into the bulk Y-123 would favour particular orientations in which the direction is parallel to *ab*-plane.

YBCO has suitable properties for ceramic materials, such as hardness and stiffness, together with tendency to fracture. However, references about the mechanical properties of this material, particularly yield strength and stress–strain curve, are scarce. The mechanical properties (hardness, Young's modulus and fracture toughness) of YBCO samples have been examined with techniques such as ultrasound,[3] X-ray diffraction[4] and nanoindentation.[5] Reported values of Young's modulus for Y-123 are within the range $E = 40$–200 GPa. This large scatter may be due to the residual porosity and poor contact between the grains.[5] Other authors,[1] also using nanoindentation, reported a value of $E = 171$–181 GPa for YBCO samples textured by the Bridgman technique, which is in agreement with Johansen,[5]

* Corresponding author.
E-mail address: joanjosep_roa@ub.edu (J.J. Roa).

0955-2219/$ – see front matter © 2009 Elsevier Ltd. All rights reserved.
doi:10.1016/j.jeurceramsoc.2009.10.021

who applied between 30 and 100 mN. Nanohardness values in the range of 7.8–8.0 GPa at maximum loads of 30 mN were recently reported by Lim and Chaudhri[6] for bulk, single-crystal YBCO. Roa et al.[1] found a hardness value of 8.9 ± 0.1 GPa by nanoindentation on YBCO samples textured by the Bridgman technique.

All these measurements were performed by sharp tips (mainly Berkovich), so an elasto-plastic regime was achieved from the beginning of the test, which yielded no information about the elasto-plastic transition. This transition can be observed if a blunt indenter is used to perform the test.

Spherical nanoindentation stress–strain curves can help us to understand elasto-to-plastic deformation in superconducting ceramics. This is relevant for the fabrication of superconducting devices at room temperature. Here we determine the elastic, plastic and elasto-plastic ranges at room temperature for YBCO samples textured by the Bridgman technique using nanoindentation with a spherical tip, and we measure the yield stress of YBCO materials by nanoindentation.

2. Experimental procedure

2.1. Preparation of bulk YBCO samples and monodomain growth

The YBCO powders were prepared by the PVA method.[7] The ratio used 69% (w/w) Y-123, 30% (w/w) Y-211 and 1% (w/w) $CeO_2{\cdot}H_2O$ was chosen to maximize critical current density.[8] The standard composition of the starting material was Y-123 with an excess of 30% (w/w) Y-211. $CeO_2{\cdot}H_2O$ was added to improve the distribution of Y-211 particles. The calcinate powder was deagglomerated by ball milling in an agate mortar.

Green bulk pieces were obtained by cold isostatic pressure (*CIP*) and further textured using the Bridgman method.[9,10] After this, bulk textured pieces were oxygenated in a horizontal furnace at 450 °C for 240 h.[11] From the oxygenated pieces all of which had a common *c*-axis tilt of 45°, small pieces of 2 mm height were cut along the *ab*-plane[12] and further polished.

2.2. Measurement of elastic properties with a spherical tipped nanoindenter

Nanoindentation tests were performed with a Nano Indenter® XP System (Agilent Technologies) with continuous stiffness measurement, CSM (harmonic displacement 2 nm and frequency of 45 Hz). The strain rate was held constant at $0.05\ s^{-1}$. The experiments were performed on the (1 0 1) plane at room temperature using a spherical diamond tip of 25 μm in radius, and performed at a maximum load of 650 mN.

In nanoindentation it is critical to correctly determine the initial contact point, especially for spherical indenters. Various methods have been used,[13] but all options require some subjectivity. For instruments with CSM capabilities, Oliver and Pharr[14] proposed, using the point at which *S* increases steadily, a method that works satisfactorily when using sharp indentations. Alternatively, they suggested using abrupt changes in CSM harmonic displacement or phase angle if they are clearer, but all options require some subjectivity.

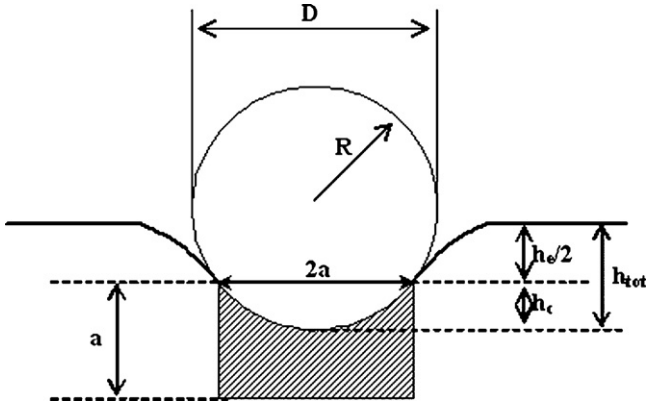

Fig. 1. Schematic representation of spherical indentation.

When using spherical tips, the contact point is more difficult to determine, due to the moderate increase in stiffness during initial contact, and the interaction between tip and sample before contacting.

Recently Barsoum et al.,[15] proposed fitting the stiffness vs. penetration depth data, and extrapolating to zero, as predicated by a relation between effective modulus and contact point, as follows[15]:

$$S = 2E_{\text{eff}}a \tag{1}$$

The stresses and deflections arising from the contact between two elastic solids are of particular interest to those undertaking indentation testing. The contact between a rigid sphere and a flat surface is shown in Fig. 1.

The mean contact pressure, p_o, is the load applied divided by the contact area. For small penetration depths, it can be obtained from the Hertzian equation[16]:

$$p_o = \frac{P}{A} = \frac{P}{\pi a^2} = \left(\frac{4E_{\text{eff}}}{3\pi}\right)\frac{a}{R}, \tag{2}$$

where P is the applied load, A is the contact area, a is the radius of the contact point, R is the radius of the tip and E_{eff} is the effective Young's modulus. Eq. (2), allows us to plot the σ–ε curves when we use the spherical nanoindentation test. The left side of this equation represents the indentation stress or mean contact pressure, also referred to as the Meyer hardness.[17] The expression in parentheses or a/R on the right side represents the indentation strain.[17]

The E_{eff} can be obtained from:

$$\frac{1}{E_{\text{eff}}} = \frac{1-\nu^2}{E} + \frac{1-\nu_i^2}{E_i}, \tag{3}$$

where ν is the Poisson's ratio, and E is the Young's modulus. The subindex i denotes the values of the indenter. For a diamond indenter, the elastic constants are $E_i = 1141$ GPa and $\nu_i = 0.07$.[18]

The radius of the circle of contact a is related to the indenter load P, the indenter radius R, and the elastic properties of the

contacting material by:

$$a = \sqrt[3]{\frac{3}{4}\frac{PR}{E_{\text{eff}}}} \tag{4}$$

The indentation load–displacement data were analysed based on the Hertz equation in the elastic region[14,19,20] as follows:

$$P = \frac{3}{4}E_{\text{eff}}R^{1/2}h_e^{3/2} \tag{5}$$

The σ–ε in a typical traction test can be written in the elastic region as:

$$\sigma = E\varepsilon, \tag{6}$$

where σ is the stress applied, E is the Young's modulus and ε is the strain. In a spherical nanoindentation, the σ–ε curves follow the same tendency; for more information see Eq. (2).

2.3. Focused ion beam sectioning

The damage produced under the residual spherical nanoindentation imprint of YBCO samples textured by the Bridgman technique was characterized using a dual beam FIB/SEM (FIB Strata DB235). The residual indentation imprints were cross-sectioned along the c-axis to evaluate the damage after indentation. A thin platinum layer was deposited on the sample prior to FIB machining in order to minimize ion-beam damage. A Ga^+ ion source was used to mill the surface at a voltage of 30 kV. The final polishing of the cross-sections was performed at 10 pA.

3. Results and discussion

Typical indentation load–displacement curves are presented in Fig. 2 for the (1 0 1)-plane orientation obtained with the 25 μm indenter. In Fig. 2a (maximum penetration depth of 100 nm), the response was elastic (the slight disagreement between the curves may be attributable to the holding time at maximum load). In Fig. 2b (maximum penetration depth of 200 nm), the response was plastic as the unload curve does not match the load curve. So, the elasto-plastic transition took place at a penetration depth of between 100 and 200 nm; the response was elastic until 150 nm

$$P = Ch_e{}^{3/2}, \tag{7}$$

after this point, the load curve can be adjusted with an elasto-plastic curve:

$$P = Ch_p{}^2. \tag{8}$$

In both equations (7 and 8, respectively) P is the applied load, C is the slope of the load curve, and h is the penetration depth. The intersection of these two curves is the yield stress of the material, which can present a pop-in event.[13]

Fig. 3 shows residual indentation imprints observed by optical microscopy. The Y-211 inclusions are heterogeneously distributed in the textured sample and this phase is not uniform below the indentation region.

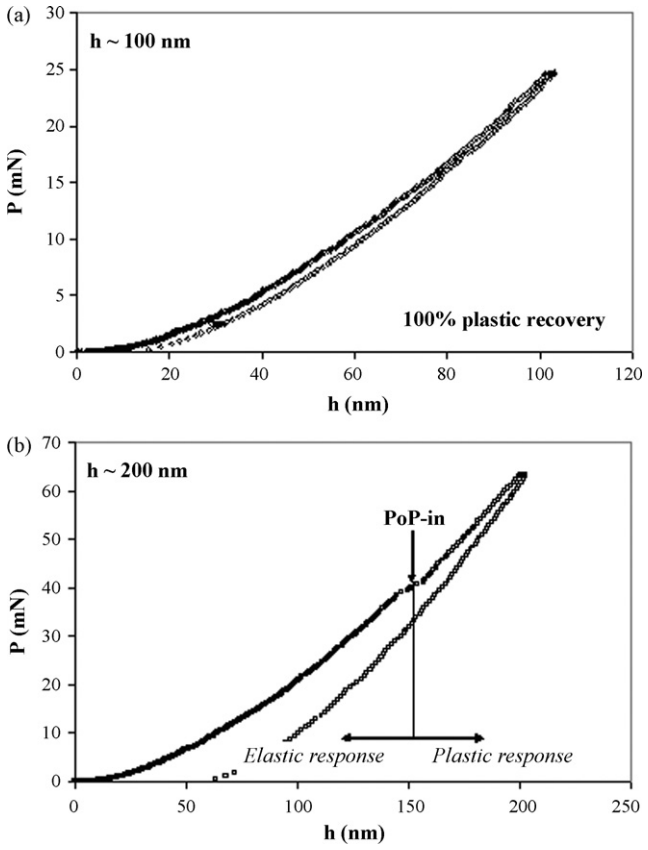

Fig. 2. Characteristic curves obtained after loading/unloading for a spherical tip indenter of 25 μm of radii at different penetration depths: (a) 100 nm, elastic response and (b) 200 nm, elastic recovery and a little plastic deformation.

An imprint is visible only by atomic force microscopy (AFM) when the test is performed at penetration depths greater than 150 nm, which correlates with the change in the slope of the loading curve due to the elasto-plastic transition (Fig. 2b). For greater penetration depths ($h > 150$ nm), different residual imprints can be observed by AFM (see Fig. 4). In Fig. 4a–c, it is seen that the Y-211 inclusions are not deformed, because this phase is harder.[1]

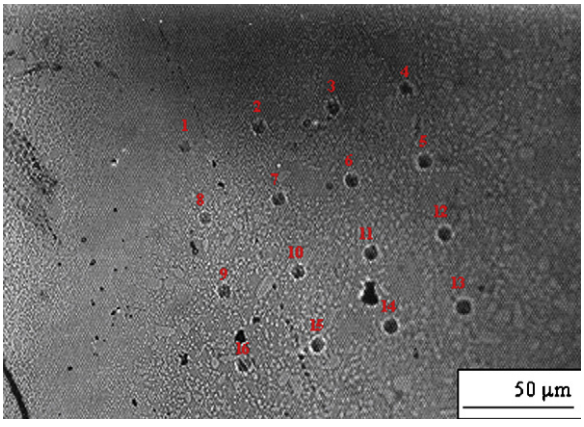

Fig. 3. Micrograph of nanoindentation imprint obtained by O.M. at an applied load of 650 mN.

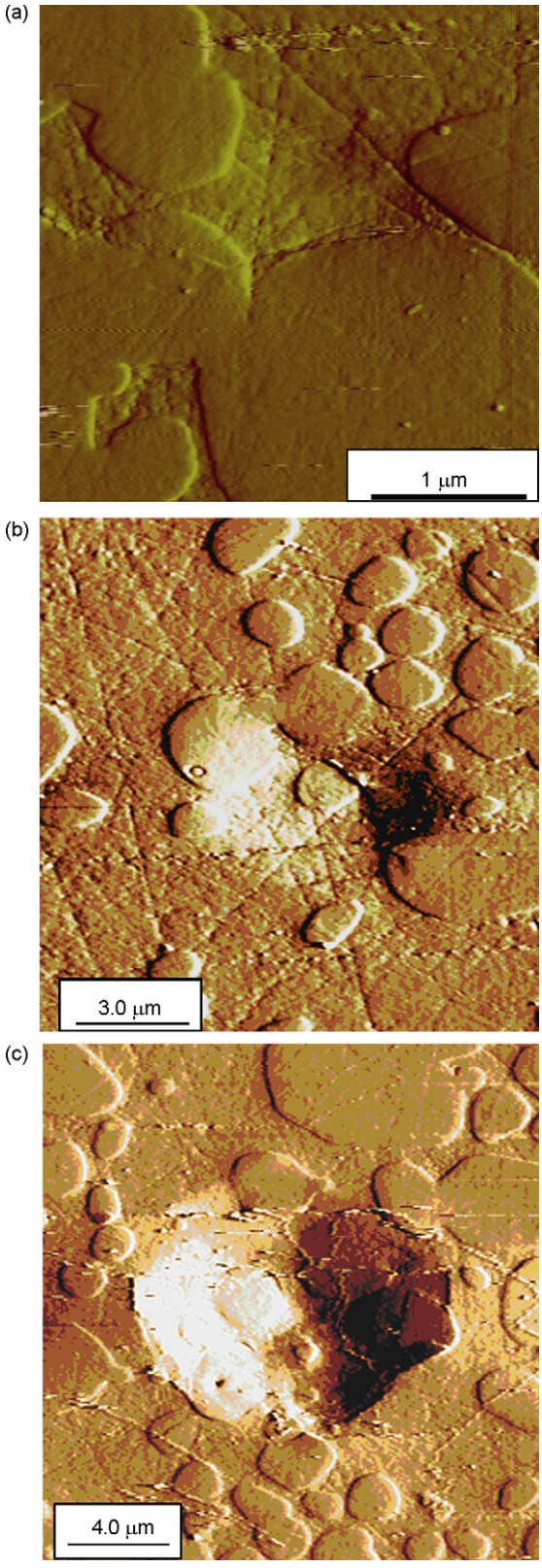

Fig. 4. AFM image at different penetration depths: (a) 300 nm, (b) 400 nm and (c) 800 nm.

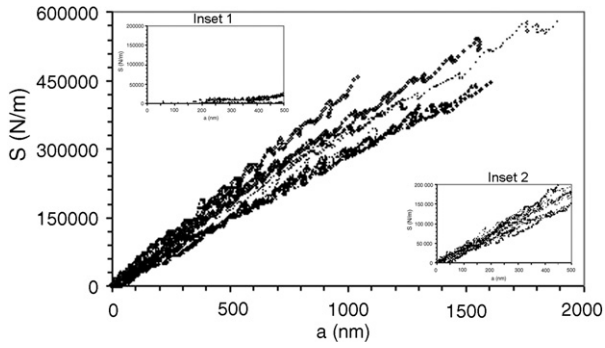

Fig. 5. Contact point (S vs. a) for samples textured by the Bridgman technique with (inset 1) elasto-plastic regimen and (inset 2) elastic regimen.

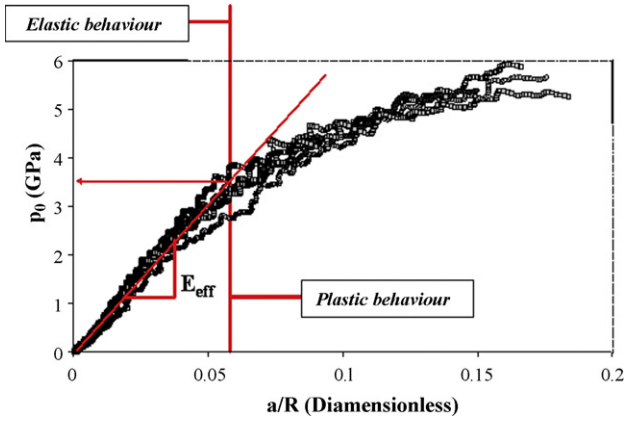

Fig. 6. Stress–strain curve textured by Bridgman technique. The solid line is the expected slope calculated from $4E_{\text{eff}}/3\pi$ (Hertzian behaviour).

For a properly zeroed sample, according to Eq. (1), a plot of S versus a should be a straight line that goes through the origin, with a slope of $2E_{\text{eff}}$. Linear regression is used to assess whether the S-versus-a curve is linear and goes through the origin. Fig. 5 shows the results of tests performed in the (1 0 1)-plane of YBCO samples textured by the Bridgman technique with the 25 μm radius indenter. The differences between the slopes presented in the S–a figure are due to the second Y-211 phase, which is not uniform under the indented region. Moreover, this phase presents a higher Young's modulus value than Y-123. However, since the tip is spherical, the single response of each phase cannot be isolated and the response of the composite is obtained (Y-123/Y-211). Inset 1 and Inset 2 in Fig. 5 shows the different tests with a bad and good contact points between the surface of the sample and the indenter. Fig. 5b plots the linear regression with a high correlation coefficient, which ensures that the contact point of the YBCO samples can be obtained correctly. After this, the Young's modulus of the material can be obtained by Hertzian equations (see Eq. (3)–(5)), giving a constant value of 123 GPa for the complete penetration range. This value is in agreement with that reported by Ledbetter et al.,[3] who obtained the E value by Ultrasonic technique and Roa et al.,[1] who used a sharp indenters. By plotting the mean contact pressure against a/R (indentation strain) it is possible to determine the point at which the elasto-plastic transition was produced. As shown in Fig. 6; the contact pressure for the elasto-plastic

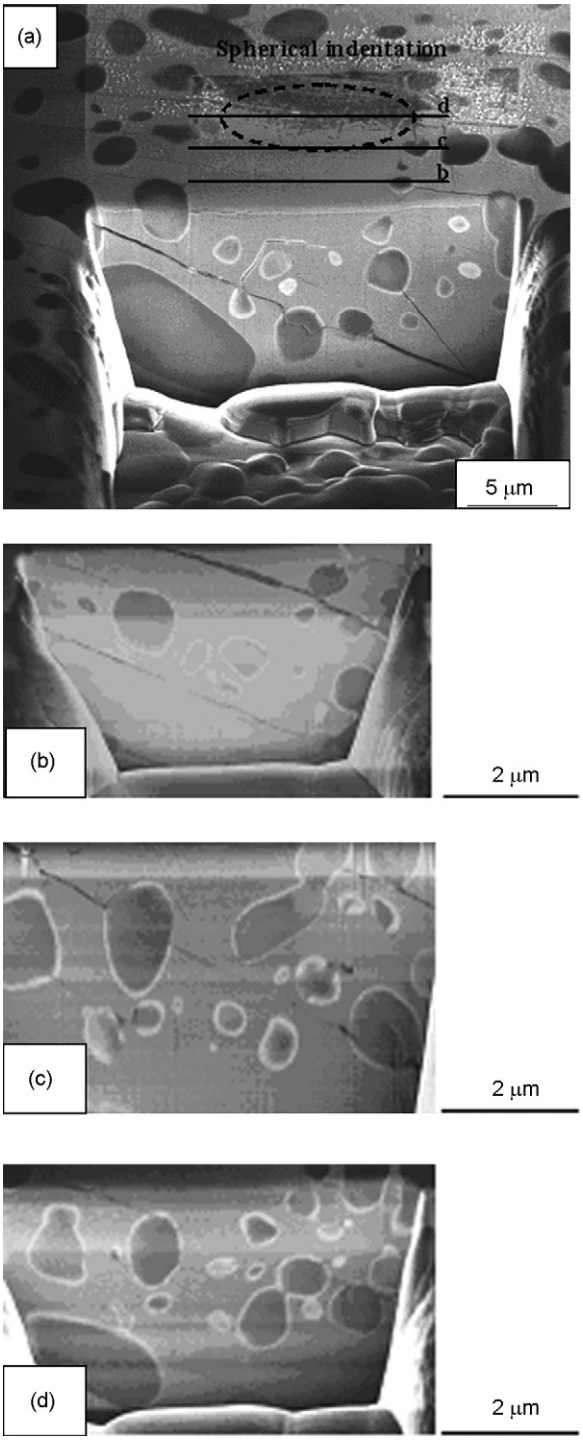

Fig. 7. Cross-sectioning and imaging of damage under indentation using the FIB-SEM: (a) indentation and platinum layer deposited on the indentation to minimize beam damage, and trench milled at high ion-beam current in front of the residual indentation imprint, (b) cross-sectioning before the imprint, (c) cross-sectioning of the border of the indentation and (d) cross-sectioning in the middle of imprint 3.

transition is 3.5 GPa (close to the hardness) beneath the indenter. There are three different regimes, which can be observed in this figure[21] depending on the contact pressure applied: (i) initially, when $p_o < 1.1\sigma_{ys}$, there is a full elastic response, and no residual impression can be observed after the removal of the applied load; (ii) $1.1\sigma_{ys} < p_o < C\sigma_{ys}$, plastic deformation occurs beneath the surface but is constrained by the surrounding elastic material, where C is a constant whose value depends on the material and the indenter geometry; (iii) finally, when $p_o = C\sigma_{ys}$ the plastic region extends to the surface of the specimen and continues to grow. One of the purposes of this work is to calculate the yield strength of YBCO samples textured by the Bridgman technique. In Fig. 6, the elasto-plastic transition can be calculated to a value of around 3.5 GPa. The value of yield stress obtained for Bridgman samples can be estimated to be 3.2 GPa.

The effect of the spherical tip indenter was examined by cross-sectioning the samples by Focused ion beams (FIB) technique. Fig. 7 illustrates the possible deformation mechanisms and the presence of cracking or porosity below the indentation imprint. First, the image shows a heterogeneous distribution of Y-211 particles around the samples, with sizes ranging from 1 to 5 μm. Also, intrinsic microcracks appear at 45° of *ab*-plane, which are generated during the tetragonal–orthorombic phase transformation. Large secondary phase inclusions (unreacted liquid and Y-211) can also create macrocraks due to thermal expansion mismatch.[22] Oxygen annealing, necessary to make Y-123 samples superconducting, is reported to be responsible for further macro and microcracking.[23] Finally, it is seen that no cracks or failure events can be appreciated under the nanoindentation imprint, indicating that the deformation can be attributed to dislocation movement or twinning of the sample, without effect of porosity or microcracking.[22] Previous studies have reported that the *ab*-plane presents a high density of dislocations. But, on the other hand, the *c*-axis presents a high quantity of twins.[2,24] Also, we believe that the plastic work produced during the indentation process contributed to closing the oxygenation crack. For this reason, we believe that the elasto-plastic transition is produced by an activation of different dislocations and twins present in the *ab*-plane and *c*-axis.

4. Conclusions

In this study we performed spherical nanoindentation tests in YBCO samples in order to examine the elastic properties and the stress–strain curves. The contact point was determined by the methodology of Barsoum et al. The following results were obtained:

(i) The Young's modulus for YBCO material was calculated with the Hertzian equations, obtaining a value of 123.5 ± 3.4 GPa. This value is in agreement with the published results obtained using sharp indentations.
(ii) The elastic-to-plastic transition occured at mean contact pressure of 3.5 GPa (at 150 nm of penetration depth) which implies that the indentation yield strength is around 3.2 GPa.
(iii) With a cross-section employing FIB technique, we showed that the samples present a heterogeneous distribution of Y-211 particles imbedded in a Y-123 matrix. No porosity or microcracking were observed, so the deformation mechanisms can be attributed to dislocations and twin generation in the *ab*-planes and *c*-axis, respectively.

Acknowledgments

We thank Dr. Y. Gaillard for assistance in AFM and Michel Barsoum and Alexander J. Moseson for helpful discussions on the determination of the contact point.

J. J. Roa acknowledges financial support from the "Comissionat per la Universitat i la Investigació del Departament d'innovació Universitari i d'Empresa de la Generalitat de Catalunya i el Fons Social Europeu".

We would also like to thank the Language Service at the University of Barcelona for linguistic and stylistic advice.

References

1. Roa JJ, Capdevila XG, Martinez M, Espiell F, Segarra M. Nanohardness and Young's modulus of YBCO samples textured by the Bridgman technique. *Nanotechnology* 2007;**18**, 385701/1.
2. Sandiumenge F, Puig T, Rabier J, Plain J, Obradors X. Optimization of flux pinning in bulk melt textured 1–2–3 superconductors. Bringing dislocations under control. *Adv Mater* 2000;**12**:375.
3. Ledbetter HM, Austin MW, Kim SA, Lei M. Elastic constants and Debye temperature of polycrystalline yttrium barium copper oxide ($YBa_2Cu_3O_{7-x}$). *J Mater Res* 1987;**2**:786.
4. Block S, Piermarini GJ, Munro RG, Wong-Ng W. The bulk modulus and Young's modulus of the superconductor $Ba_2Cu_3YO_7$. *Adv Ceram Mater* 1987;**2**:601.
5. Johansen TH. Flux-pinning-induced stress and magnetostriction in bulk superconductors. *Supercond Sci Technol* 2000;**13**:R121.
6. Lim YY, Chaudhri MM. Nanohardness mapping of the curved surface of spherical macroindentations in fully annealed polycrystalline oxygen-free copper. *Phys Status Solidi A: Appl Res* 2002;**194**(1):19–29.
7. Serradilla IG, Calleja A, Capdevila XG, Segarra M, Mendoza E, Teva J, et al. Synthesizing the Y-123/Y-211 composite by the PVA method. *Supercond Sci Technol* 2002;**15**:566.
8. Piñol S, Gomis V, Martinez B, Labarta A, Fontcurberta J, Obradors X. Bridgman growth and enhanced critical currents in textured yttrium barium copper oxide. *J Alloys Compd* 1993;**195**:11.
9. Granados X, Piñol S, Martín B, Galante F, Sandiumenge F, Fontcuberta J, et al. Direccional solidification of YBCO rods for current lead applications. *Cryogenics* 1994;**34**:833.
10. Piñol S, Obradors X, Martín B, Fontcuberta J, Sandiumenge F. Patent ES-2111435.
11. Tournier RF, Bourgault D, Buzon D, Chaud X, Folch E, Isfort D, et al. $YBa_2Cu_3O_{7-x}$ single domain growth and shaping for fault current limiting applications. *Adv Sci Technol* 2003;**38**:3.
12. Ullrich M, Leenders A, Krelaus J, Kautschor L-O, Freyhardt HC, Schmidt L, et al. High temperature deformation of Bridgman melt-textured YBCO. *Mater Sci Eng* 1998;**B53**:143.
13. Basu S, Barsoum MW. Deformation micromechanisms of ZnO single crystals as determined from spherical nanoindentation stress–strain curves. *J Mater Res* 2007;**22**:2470.
14. Oliver WC, Pharr GM. Measurement of hardness and elastic modulus by instrumented indentation: advances in understanding and refinements to methodology. *J Mater Res* 2004;**19**:3.
15. Moseson AJ, Basu S, Barsoum MW. Determination of the effective zero point of contact for spherical nanoindentation. *J Mater Res* 2008;**23**: 204.
16. Jiménez-Piqué E, Gaillard Y, Anglada M. Instrumented indentation of layered ceramic materials. *Key Eng Mater* 2007;**333**:107.
17. Basu S, Moseson A, Barsoum MW. On the determination of spherical nanoindentation stress–strain curves. *J Mater Res* 2006;**21**:2628.
18. Oliver WC, Pharr GM. An improved technique for determining hardness and elastic modulus using load and displacement sensing indentation experiments. *J Mater Res* 1992;**7**:1564.
19. Field JS, Swain MV. A simple predictive model for spherical indentation. *J Mater Res* 1993;**8**:297.
20. Field JS, Swain MV. Determining the mechanical properties of small volumes of material from submicrometer spherical indentations. *J Mater Res* 1995;**10**:101.
21. Fisher-Cripps AC. *Nanoindentation*. 2nd ed. New York, United States of America: Springer-Verlag Press; 2004. pp. 3, 9–10.
22. Gaillard Y, Jiménez-Piqué E, Soldera F, Mücklich F, Anglada M. Quantification of hidrotermal degradation in zirconio by nanoindentation. *Acta Mater* 2008;**56**:4206.
23. Isfort D, Chaud X, Tournier R, Kapelski G. Cracking and oxygenation of YBaCuO bulk superconductors: application to *c*-axis elements for current limitation. *Physica C* 2003;**390**:341.
24. Diko P, Gawalek W, Habisreuther T, Klupsch T, Gornert P. Macro- and microcracking, subgrains, twins and thermal stresses in $YBa_2Cu_3O_{7-x}$ (123)-Y_2BaCuO_5 (Y211) melt-textured superconductors studied by means of polarized light microscopy. *J Microsc* 1996;**184**:46.